Energetics of Al doping and intrinsic defects in monoclinic and cubic zirconia: First-principles calculations

C. Århammar,[1,2] C. Moysés Araújo,[2] and Rajeev Ahuja[1,2]
[1]*Applied Materials Physics, Department of Materials and Engineering, Royal Institute of Technology (KTH), S-100 44 Stockholm, Sweden*
[2]*Condensed Matter Theory Group, Department of Physics and Materials Science, Uppsala University, P.O. Box 530, S-751 21 Uppsala, Sweden*

(Received 2 January 2009; revised manuscript received 10 August 2009; published 18 September 2009)

First-principles theory within the supercell approach has been employed to investigate Al doping and intrinsic defects in monoclinic and cubic zirconia. The effect of oxygen chemical potential and Fermi level on the formation energy and on the defect concentration have been taken into account. The formation of oxygen vacancies is found to be energetically more favorable in the cubic than in the monoclinic phase under the same oxygen chemical potential and Fermi energy. In both phases, substitutional Al decays from neutral charge state into the charge state −1, with the transition energy just above to the top of the valence band. Our findings indicate that by confining the Fermi energy to the region between the middle of the band gap and the bottom of the conduction band, high Al solubility could be achieved, although formation of Al is likely followed by the formation of interstitial oxygen. Furthermore, the concentration of Al with charge state −1 along with the equilibrium Fermi energy have been calculated in a self-consistent procedure. Here, the possible compensating defects with the relevant charge states have been considered. The obtained concentrations of Al and oxygen vacancies follow the experimental trend but underestimates experimental data. When the formation of defect clusters, composed by two substitutional Al and one oxygen vacancy, are considered, good quantitative agreement with experimental values of both Al and oxygen vacancy concentration is achieved. The results suggest that defect clusters will be formed as a result of Al doping in cubic phase of ZrO_2, whereas the concentration of defect clusters is negligible in the monoclinic phase, both in accordance with experiment.

DOI: 10.1103/PhysRevB.80.115208 PACS number(s): 61.72.uf, 61.72.uj, 71.55.−i

I. INTRODUCTION

Among others, zirconia (ZrO_2) is a promising candidate as a gate dielectric material in metal-oxide-semiconductor transistors and is one of the most popular electrolytes for use in fuel cells.[1,2] Furthermore, its excellent mechanical properties makes ZrO_2 suitable in protective coating applications. The monoclinic phase of ZrO_2 is stable in the temperature range from room temperature up to about 1150 °C, when the tetragonal phase is formed. At around 2370 °C the system undergoes a phase transformation to the cubic phase, which is stable up to the melting point at 2680 °C. Common oxides used to stabilize tetragonal and cubic phases of ZrO_2 are MgO, Y_2O_3, CaO, and Ce_2O_3. It has been generally recognized that the doping with cations, displaying lower valence than Zr, introduces oxygen vacancies into the crystal lattice and that the cubic phase has a high degree of oxygen under stoichiometry (61–66.7 at. % O), compared to the nearly stoichiometric monoclinic phase.[3] In addition, the molar volume of ZrO_2 increases from cubic to tetragonal and monoclinic phase, leading to so-called transformation toughening. This toughening behavior is useful in cutting tool applications, where oxides are used as coatings on cemented carbides.[4]

Al_2O_3 has since long served as one of the most important coating materials on metal cutting tools.[5] Composites of Al_2O_3 and ZrO_2 display large versatility due to formation of different phases and variation in microstructure. Trace addition of Al_2O_3 into ZrO_2 and composite formation of Al_2O_3 and ZrO_2 show increased hardness and fracture toughness with respect to single phases.[6] Moreover, Zr has shown to have a strong effect on texture and growth of coatings of Al_2O_3 and Al has proved significant effect on the phase composition and growth of ZrO_2.[5,7] It is not well known whether the properties of these composites are related to the combined properties of the pure phases (the composite) or to effects of solubility of Zr into Al_2O_3 and/or of Al into ZrO_2. In the monoclinic phase of ZrO_2, a recent thermodynamic study shows no solubility of Al,[8] whereas another study found a small solubility of 0.7 ± 0.3 mol %.[9] In the tetragonal phase, however, solubilities generally range from 7 to 8.7 mol %.[10] By synthesizing a solid solution of Al_2O_3 and ZrO_2 from solution instead of from mixing of powders, the solid solution of Al in tetragonal phase can be considerably higher. Solubilities of Al into tetragonal ZrO_2 of up to 10 mol %, forming the crystalline so-called t' phase, with c/a ratio >1 and even above 10% forming t'' phase with $c/a=1$ have been achieved by this method.[11] With similar methods, Stefanic *et al.*[12] have achieved up to 50 mol % of Al in the t' phase.

Current experimental data does not provide a detailed fundamental understanding of the Al solubility in ZrO_2. In order to fill this gap of knowledge, atomistic modeling is a suitable approach. Despite the great technological importance of this system, no theoretical studies by first-principles theory have been carried out, neither to understand the solubility of Al in ZrO_2 nor to investigate the intrinsic defects in the high-temperature phases of ZrO_2. To the best of our knowledge, only the formation of intrinsic defects in monoclinic phase of ZrO_2 has been subject of study for first-principle theory.[1,2,13]

It should be pointed out that these theoretical studies have provided valuable complementary information to experimental findings. Our aim is to access the energetics of Al doping and intrinsic defect formation in different phases of ZrO_2. More specifically, we have investigated the solid solution of Al at interstitial and substitutional positions and the formation of O and Zr vacancies and interstitials in the monoclinic and cubic phase of ZrO_2 by the means of first-principles theory.

The paper is structured as follows: first, the results for the pristine systems are presented and the formalism of defect formation energy and the necessary corrections for defect-defect interactions and density-functional theory (DFT) band-gap (BG) underestimation are introduced. Second, the defect sites and coordination are briefly discussed. Thereafter we present formation energies of the relevant neutral and charged defects. The self-consistent Fermi energy (FE) of both defect-containing phases, at different experimental conditions, is calculated and from this we derive the equilibrium Al and oxygen vacancy concentration. Finally, the interaction between defects is investigated and two routes to increase Al solubility are presented.

II. COMPUTATIONAL METHOD

The calculations were performed within the framework of the generalized gradient approximation (GGA)[14] to density-functional theory by using the projected augmented wave (PAW) method[15] and the GGA-PW91 functional,[16] as implemented in the Vienna *ab initio* simulation package (VASP). The PAW potentials included the valence states $4s^2 4p^6 4d^2 5s^2$ for Zr, $2s^2 2p^4$ for O, and $3s^2 3p^1$ for Al. To overcome energy barriers, molecular-dynamics simulations using the VASP code were performed at 573 K for some of the investigated defects. For the defect-free structures, we used k-point grids resulting in 13 and 36 k-points in the irreducible Brillouin zone (IBZ) for the cubic and monoclinic ZrO_2, respectively. We have used a cutoff energy of 750 eV in both cases, resulting in a well converged total energy (less than 10 meV). We have also performed calculations on the hexagonal phase of Al_2O_3, α alumina, using a 30-atom-sized cell. Here we have used a k points mesh resulting in 34 k points in the IBZ and an energy cutoff of 750 eV. From the pristine unit cells of ZrO_2, we have built up $2\times2\times2$ supercells containing 96 atoms for monoclinic phase ($p2_1c$) and 81 atoms for cubic phase ($Fm\bar{3}m$).[17] Here, we have used an energy cutoff of 520 eV, resulting in a total-energy convergence of less than 60 meV and a $2\times2\times2$ k-point grid for the three phases of ZrO_2. This was found sufficient since the total-energy difference between the $2\times2\times2$ and $4\times4\times4$ grids was less than 1 meV. We investigated the formation energy convergence with supercell size, by considering 1 Al atom at a substitutional position in two sizes of supercells, 96 and 12 atoms of monoclinic phase of ZrO_2. These sizes correspond to concentrations of 1 and 8 at. %. The difference in defect formation energy between the two systems was only 40 meV, indicating that the 96 atoms supercell is large enough to achieve converged formation energies. As reference systems, hcp Zr, fcc Al, and molecular oxygen has been used. The convergence of k points and cutoff of hcp Zr and fcc Al was carefully checked, resulting in a cutoff of 520 eV and 52 k points in the IBZ of hcp Zr. For fcc Al, the energy cutoff was chosen to be 600 eV and 28 k points in the IBZ, which was enough to converge the total energy to less than 10 meV. All structures were optimized without using any symmetry constraint. Spin-polarized calculations were performed for all defect-containing supercells. For all cases, but the Zr vacancy, the magnetic moment turned to $0\mu_B$ after relaxation of the supercell, indicating that all other defects are nonmagnetic.

To investigate the formation of intrinsic and extrinsic defects, we have employed a formalism where the formation energy is defined as[13,18,19]

$$\Delta H_f(D^q, E_F, \mu) = [E_T(D^q) - E_T(H)] - \sum_\alpha n_\alpha(\mu_\alpha^{elem} + \Delta\mu_\alpha) + q(\Delta E_F + E_V). \quad (1)$$

The first two terms, $E_T(D^q)$ and $E_T(H)$, are the total energies of the supercells with and without defect, respectively. In the third term, n_α is the number of atoms added ($n_\alpha>0$) or removed ($n_\alpha<0$) to create the defect while $\mu_\alpha=\mu_\alpha^{elem}+\Delta\mu_\alpha$ is the chemical potential of the reservoir containing α atoms ($\alpha\equiv$Zr, O, and Al). In order to keep thermodynamic equilibrium between the components, Zr and O, and the target compound of our study, ZrO_2, the relation $2\Delta\mu_O+\Delta\mu_{Zr}=\Delta H_f(ZrO_2)$ should be satisfied, where $\Delta H_f(ZrO_2)$ is the calculated formation energy of zirconia. Thus, the atomic chemical potentials can be chosen between the limits of O-rich [Zr-poor, $\Delta\mu_O=0$ and $\Delta\mu_{Zr}=\Delta H_f(ZrO_2)$] and O-poor [Zr-rich, $\Delta\mu_{Zr}=0$ and $\Delta\mu_O=\frac{1}{2}\Delta H_f(ZrO_2)$] conditions. These atomic chemical potentials are variables in this formalism, controlled by the experimental conditions. The chemical potential of Al could, in principle, change from minus infinity (which represents total absence of this atomic species in the growth environment) up to that of solid Al metal. However, Al may react with O to form Al-O compounds, which work as solubility-limiting phases. Therefore, one should control the Al chemical potential in order to avoid precipitation of undesired phases. In this work, we have used the constraint $\Delta\mu_{Al}\leq\frac{1}{2}(\Delta H_f(Al_2O_3)-3\Delta\mu_O)$. The last term in Eq. (1) accounts for a change in the defect charge state. Here, q is the charge state of the defect (for neutral defects, $q=0$) and $E_F=\Delta E_F+E_V$ is the Fermi energy referenced to the valence-band maximum (VBM) of the defect-free supercell, E_V.

We will now describe the corrections to the formation energy, which were performed in this work. The Fermi energy was referenced to the VBM calculated in the defect-free supercell and a potential alignment correction term was added for a few test cases. There are alternate ways to calculate this correction term.[18–20] We used the method of aligning the eigenvalues of the localized O $2s$ states of an oxygen far away from the defect in the defect supercell with the O $2s$ states of an oxygen at the same position in the intrinsic system. We have found that the alignment was small enough (<0.2 eV) to have no effect on the charge state transitions and it was then not further used. The unphysical charge image interactions were corrected by the method of Makov-Payne (MP).[21] Since charged defects were studied in this

TABLE I. Cell parameters and volume for intrinsic ZrO_2 and Al_2O_3.

	a (Å)	b (Å)	c (Å)	V (Å^3/f.u.)
Monoclinic ZrO_2	5.208	5.285	5.389	36.619
Ref. 23	5.1454	5.2075	5.3107	36.85
Ref. 17	5.234	5.238	5.396	36.22
Cubic ZrO_2	5.146	5.146	5.146	34.06
Ref. 24	5.164	5.164	5.164	34.44
Ref. 25	5.086	5.086	5.086	32.89
Hexagonal Al_2O_3	4.787	4.787	13.071	43.23
Ref. 26	4.7620	4.7620	12.986	
Ref. 27	4.763	4.763	13.003	

work, the size of the band gap is of great importance. To correct for the DFT underestimation of the fundamental band gap, we shifted the conduction band (CB) upward in energy by ΔE_g in order to match the experimental band gap of 5.83 eV (6.1 eV) for monoclinic (cubic) phase.[22] We have used ΔE_g=3.34(2.42) eV for the monoclinic (cubic) structure. Then, we assume that shallow donor states shift linearly with the expansion of the band gap and estimate the shift of ΔH_f of these donors by an amount given by $\Delta E^{D^q}=n\Delta E_g$, where n is the number of donors states. The accuracy of this approach will depend on how large the many-body contribution to the total energy is. For further information on the above-mentioned corrections to the supercell approach we recommend the articles of Van de Walle[19] and Persson.[18]

III. RESULTS

A. Pristine systems

The formation energies of monoclinic and cubic ZrO_2 as well as of hexagonal Al_2O_3 were calculated by taking the ground-state elemental metals and O_2 total energies as reference for which we have found the values of −10.43, −10.23, and −15.82 eV per formula unit (f.u.), respectively. These values are in reasonable agreement with the corresponding experimental values of −11.68, −11.26, and −17.44 eV per f.u. for the monoclinic, cubic ZrO_2, and hexagonal Al_2O_3, respectively,[8] and in good agreement with other theoretical works, where the energy difference between monoclinic and cubic phase is calculated in Ref. 2 to the value of −0.17 eV per f.u. and the formation energy of monoclinic phase is calculated in Ref. 13 to the value of −10.662 eV per f.u. The difference in formation energy between our calculated value for ZrO_2 and that of Zheng *et al.* is most likely due to the calculation of the binding energy of the oxygen molecule. Our calculated binding energy of 5.12 eV for the O_2 molecule compares well to the experimental value of 5.17 eV.[23] The calculated cell parameters are in good agreement with experimental data, as seen in Table I. The structures of pristine monoclinic and cubic phase of ZrO_2 and of hexagonal phase of Al_2O_3 are shown in Fig. 1.

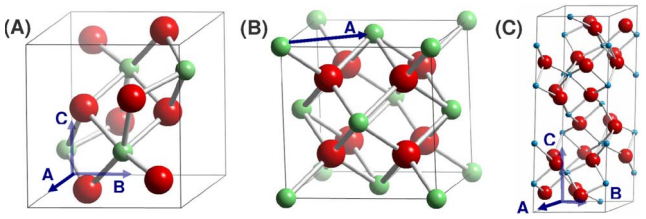

FIG. 1. (Color online) The structures of (a) monoclinic phase, (b) cubic phase of ZrO_2, and (c) hexagonal phase (corundum structure of Al_2O_3). Oxygens are displayed as large, red atoms, zirconium as small green atoms, and aluminum as small blue atoms.

B. Defect sites

The size of ionic Al is very small (Pauling ionic radius 50 pm for Al^{3+}), as compared to ionic Zr (Pauling ionic radius 80 pm for Zr^{4+}), thus it is important to consider interstitial positions besides substitutional doping. Furthermore, experiments support the existence of interstitial Al at high concentrations.[11,12] Therefore, calculations were performed for interstitial Al, and for completeness, also for interstitial Zr and O in both phases of ZrO_2. The positions of these interstitials and of the substitutional defects in monoclinic zirconia are displayed in Fig. 2. In monoclinic ZrO_2, we found an oxygen interstitial, initially situated at a position with the fractional coordinates (0.10 0.92 0.80), forming a "dumbbell" pair with a nearest-neighbor fourfold Zr-coordinated lattice oxygen after relaxation. The O-O bond distance between the interstitial and the fourfold Zr-coordinated lattice oxygen was found to be 1.5 Å (Fig. 3). This oxygen interstitial is identical to the one binding to a fourfold Zr-coordinated lattice oxygen (denoted as O_4),

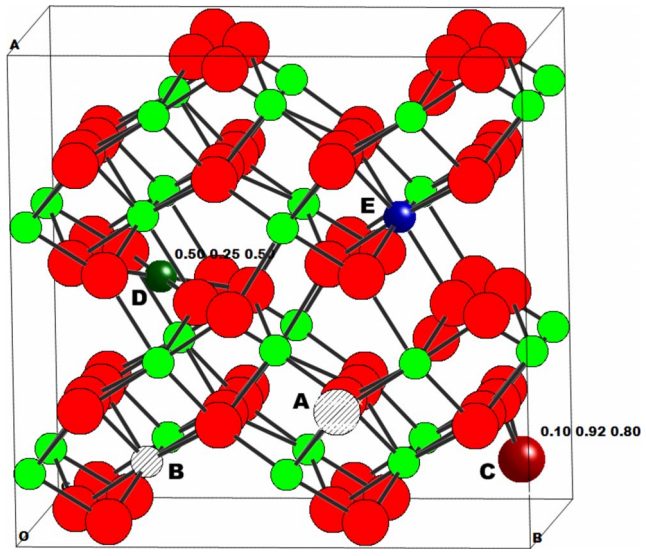

FIG. 2. (Color online) An illustration of the investigated defects in monoclinic phase of ZrO_2: (a) oxygen vacancy, (b) Zr vacancy, (c) oxygen interstitial, (d) Zr/Al interstitial, and (e) Al substitutional. Oxygens are displayed as large, red atoms, zirconium as small, green atoms, and aluminum as small, blue atoms. Interstitials are rendered and vacancies are dashed. The initial positions of the Zr/Al and O_4 interstitial are displayed as bold labels at the defect sites.

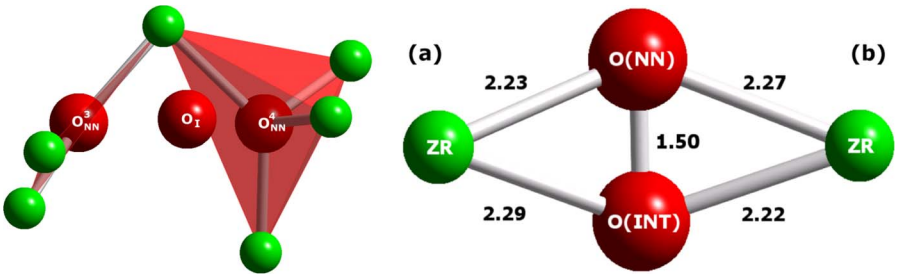

FIG. 3. (Color online) Coordination of the fourfold oxygen interstitial in monoclinic ZrO_2 (a) before and (b) after relaxation. Oxygens are displayed as large, red atoms and zirconium as small, green atoms.

found by Foster *et. al.*[1,2] We also considered the oxygen interstitial being nearest neighbor to the threefold Zr-coordinated lattice oxygen, denoted as O_3 by Foster *et al.*[1,2] We then displaced the oxygen interstitial, closer to the threefold-coordinated lattice oxygen, at the position with fractional coordinates (0.08 0.91 0.02). At 0 K, we have not found any stable energy minimum when relaxing without any symmetry constraints. Therefore, molecular-dynamics simulations at 573 K were performed in order to overcome energy barriers. After thermalizing at this temperature, we quenched to 0 K and achieved an energy minimum. This energy is slightly lower (20 meV) than the energy of the fourfold interstitial but we do not observe the significant difference in energy between the two interstitials as is observed by Foster *et al.*[1,2] This conflicting result might be due to a strong dependence on initial position of the oxygen interstitial. Since the radius of the oxygen interstitial is quite large there might be high kinetic barriers, limiting diffusion from one site to another.

For the formation of oxygen vacancies there are two positions in the monoclinic structure where oxygen is either threefold or fourfold coordinated (V_{O3} and V_{O4}). We have investigated the energetics of both defect sites and found that the threefold-coordinated vacancy was lower in energy, using the GGA-PW91 functional. Foster *et al.*[1,2] use the GGA-PW91 functional and states that the main properties of the three- and four-coordinated oxygen vacancy are very similar and therefore they only discuss the fourfold vacancy. Furthermore, Zheng *et al.* uses the GGA-PBE functional and calculates the formation energy and charge state transitions of V_{O3} and V_{O4}, finding V_{O4} slightly lower in energy, 0.11 eV. In order to investigate the effect of the choice of functional, we tried using the Perdew, Burke and Ernzerhof (GGA-PBE)[23] functional, calculating the total energy of V_{O3} and V_{O4}. We found very good agreement with Zheng *et al.*,[13] with an energy difference between V_{O3} and V_{O4} of 0.11 eV. Thus, we conclude that the choice of functional does have a significant effect on the stability of the intrinsic defects in ZrO_2. Since the GGA-PW91 provides the lowest formation energies for both the neutral V_{O3}, V_{Zr}, and O_4 in comparison with the available literature, we have chosen this functional throughout this work. The cation and oxygen vacancy position in cubic phase of ZrO_2 are both unique and can thus readily be determined. The lowest energy cation interstitial position was found to be octahedrally coordinated at the position with fractional coordinates $(\frac{1}{2}\ \frac{1}{4}\ \frac{1}{2})$. In similarity with the monoclinic phase, the oxygen interstitial in cubic phase also forms a bond with a fourfold Zr-coordinated lattice oxygen, at a O-O bond distance of 1.49 Å. The interstitial cation position in cubic phase is at exactly $(\frac{1}{2}\ \frac{1}{2}\ \frac{1}{2})$, coordinated with six oxygens.

C. Defect formation energies

Now we turn to the analysis of the most relevant neutral and charged defects. Here, two different oxygen chemical potentials, oxygen-poor (O-poor) and oxygen-rich (O-rich) conditions were investigated. In Table II, we display the formation energies at $E_F=E_V$ of the following defects in different charge states in monoclinic and cubic phase of ZrO_2: Al substitutional (Al_{Zr}) and interstitial (Al_i); Zr interstitial (Zr_i) and vacancy (V_{Zr}); and O interstitial (O_3 and O_4) and vacancy (V_{O3} and V_{O4}). An illustration of these defects in the cubic phase of ZrO_2 are displayed in Fig. 3. Al^0_{Zr} displays the lowest formation energy under O-rich conditions (the formation energy is decreased to about half of its value) while Al^0_i is favored under O-poor conditions, this follows from the constraint to avoid Al_2O_3 formation. Al^0_i is high in energy compared to Al^0_{Zr} and the formation energy of Al_{Zr} and Al_i is higher in energy in cubic phase than in monoclinic phase. Our results for oxygen-related defects in the monoclinic phase are in good agreement with those of Refs. 1, 2, and 13. Our formation energies of the neutral and charged O_4 are lower than that of Foster *et al.*, whereas the formation energy of neutral O_3 is higher than their values. We find an O_3 formation energy of 1.99 eV, whereas Zheng and Foster *et al.*[1,2,13] find values of 1.31 and 1.4 eV, respectively. In cubic phase, O_4 is higher in energy than in monoclinic phase. This is most probably due to the higher density of the cubic structure as compared to the monoclinic, limiting mobility of the oxygen ion. O^0_4 has lower formation energy under O-rich conditions (2.02 eV), Foster *et al.* find a value of 2.2 eV, whereas V^0_{O3} displays the lowest formation energy of all neutral defects, 0.82 eV for monoclinic and 0.23 eV for cubic phase, under O-poor conditions. Zheng *et al.* find a value of 0.93 eV for monoclinic phase at the same conditions. This low formation energy of V_{O3} corroborates with the experimentally observed under stoichiometry in cubic ZrO_2.[28] At oxygen-rich conditions our calculated formation energy of V_{O3} is lower than both those of Zheng and Foster *et al.* Later in this paper, we will show that despite the low V^0_{O3} formation energy in monoclinic phase, the equilibrium concentration of V^0_{O3} will still be low in the temperature range where monoclinic phase is stable. V^0_{Zr} is favored under O-rich con-

TABLE II. Formation energies at $E_F=E_V$ for the various defects in ZrO_2. Units are in eV/defect. Data are without any corrections. In parentheses are data from Ref. 13 and in brackets are data from Ref. 2.

			Monoclinic ZrO_2		Cubic ZrO_2	
Defect	Charge on defect	Kroger-Vink notation	$\Delta\mu_O=0$	$\Delta\mu_{Zr}=0$	$\Delta\mu_O=0$	$\Delta\mu_{Zr}=0$
V_{O3}^{0}	0	V_{O3}^{X}	5.88(6.26), [8.90]	0.66(0.93)		
V_{O3}^{-1}	−1	$V_{O3}^{\cdot}$	10.23	5.02		
V_{O3}^{-2}	−2	$V_{O3}^{\cdot\cdot}$	13.72	8.51		
V_{O3}^{+1}	+1	$V_{O3}^{\prime}$	3.96(3.54)	−1.26(−1.79)		
V_{O3}^{+2}	+2	$V_{O3}^{\prime\prime}$	0.88(0.54)	−4.33(−4.79)		
V_{O4}^{0}	0	V_{O4}^{X}	6.63(6.15), [8.88]	1.42(0.82)	5.35	0.23
V_{O4}^{-1}	−1	$V_{O4}^{\cdot}$			9.43	4.32
V_{O4}^{-2}	−2	$V_{O4}^{\cdot\cdot}$			12.69	7.57
V_{O4}^{+1}	+1	$V_{O4}^{\prime}$			3.04	−2.08
V_{O4}^{+2}	+2	$V_{O4}^{\prime\prime}$			−1.19	−6.30
V_{Zr}^{0}	0	V_{Zr}^{X}	5.74(5.78)	16.16(16.44)	3.65	13.88
O_3^{0}	0	O_3^{X}	1.99(1.31)	7.20(6.64)		
O_4^{0}	0	O_4^{X}	2.02[2.2]	7.23	2.49	7.61
O_4^{-1}	−1	$O_4^{\cdot}$	3.73[3.9]	9.04	4.17	9.38
O_4^{-2}	−2	$O_4^{\cdot\cdot}$	4.43[5.3]	10.03	4.53	10.02
O_4^{+1}	+1	$O_4^{\prime}$	1.73	7.05	2.67	7.88
O_4^{+2}	+2	$O_4^{\prime\prime}$	1.67	7.27	2.74	7.85
Zr_i^{0}	0	Zr_i^{X}	14.32(14.28)	3.89(3.61)	12.74	2.51
Al_{Zr}^{0}	0	Al_i^{X}	1.64	4.25	3.38	5.94
Al_{Zr}^{-1}	−1	$Al_i^{\cdot}$	1.70	4.31	3.48	6.04
Al_{Zr}^{-2}	−2	$Al_i^{\cdot\cdot}$	6.24	8.85	6.71	9.27
Al_{Zr}^{-3}	−3	$Al_i^{\cdot\cdot\cdot}$	9.76	12.36	9.87	12.43
Al_i^{0}	0	Al_i^{X}	10.93	3.11	14.10	6.43
Al_i^{+1}	+1	$Al_i^{\prime}$	8.57	0.68	12.02	4.35
Al_i^{+2}	+2	$Al_i^{\prime\prime}$	6.51	−1.23	8.26	0.59
Al_i^{+3}	+3	$Al_i^{\prime\prime\prime}$	4.94	−2.88	6.14	−1.53

ditions, which follows from the conditions of thermodynamic equilibrium with ZrO_2. Zr_i^0 will display the highest equilibrium concentration under O-poor conditions in ZrO_2 but is higher in energy compared to the other intrinsic defects, as is V_{Zr}^0.

The formation energies of the intrinsic defects, as well as Al interstitial and substitutional dopants as a function of Fermi energy are presented in Figs. 4(a)–4(d). We display only the lowest energy charge state at a given Fermi energy. In dashed lines, the uncorrected formation energies for V_{O3} are shown in order to compare with Refs. 1, 2, and 13. The corrected formation energies of all investigated defects are shown in solid lines. We focus our interest on the Al- and O-related defects and do not take Zr interstitials or vacancies into account since they are the highest in energy of all intrinsic defects. Let us first describe the result for the intrinsic defects in monoclinic phase, Figs. 4(a) and 4(b). Without corrections, V_{O3} displays two transitions, $(+2|0)$ and $(0|-2)$, at FEs of 2.50 and 3.91 eV, respectively. The picture changes dramatically as the band-gap correction is added, shifting the negative charge states as well as the neutral state to higher energies, thus increasing the stability range of V_{O3}^{+2}. Our corrected V_{O3} stability ranges differ from those of Zheng *et al.*[13] This is due to two facts. First, Zheng *et al.*[13] have not performed a band-gap correction. This is clear since our results are identical to theirs up to the neutral stability region. Second, they have not considered negative charge states. Several authors have suggested that oxygen vacancies can occur in negative charged states.[2,29] Nevertheless, the negative charge states will be too high in energy to be stable if the band-gap correction is applied. In cubic phase, Figs. 4(c) and 4(d), the V_{O3} displays two transitions $(+2|0)$ and $(0|-2)$ at FEs of 3.27 and 3.67 eV, respectively. In similarity with monoclinic phase, the charge states of V_{O3} are shifted to higher energies as we apply the band-gap correction. Our results for O_4 in monoclinic phase are in close agreement with the results for O_3 of Zheng *et al.*[13] (where only the charge state transitions of the three-coordinated interstitial are displayed), with one transition $(0|-2)$ at a FE of 1.44 eV, turning to negative values at around a FE of 5.20 (2.40) eV under oxygen-poor (oxygen-rich) conditions. In cubic phase O_i displays the transition $(0|-2)$ at a FE of 1.40 eV and turns

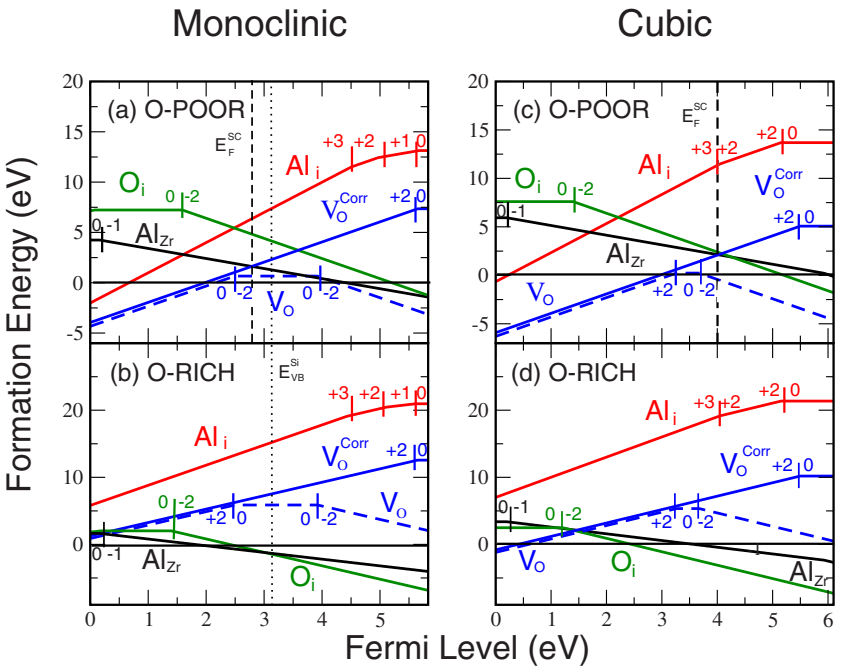

FIG. 4. (Color online) Defect formation energy as a function of Fermi energy for (a) monoclinic phase under O-poor conditions, (b) monoclinic phase under O-rich conditions, (c) cubic phase under O-poor conditions, and (d) cubic phase under O-rich conditions. The maximum value of the x axis is set to the experimental band gap from Ref. 22. Uncorrected formation energies for threefold Zr-coordinated oxygen vacancies are displayed with dashed lines and corrected formation energies for all defects are displayed by solid lines. The self-consistent Fermi Energy at 1100 K is displayed as vertical dashed lines. The VBM of Si with respect to monoclinic ZrO_2 is displayed as a vertical dotted line.

into negative formation energies at a FE of 5.19 (2.46) eV. In Fig. 5, the density of states (DOS) of monoclinic ZrO_2, containing O_4 defects is shown. As can be seen from DOS, neither one of the O_4 charge states in monoclinic phase interact with the CB. The same is observed in cubic phase (not shown here).

Now, we discuss the Al substitutional and interstitial defects. As can be observed in Figs. 4(a)–4(d), Al_{Zr} undergoes one transition $(0|-1)$ at a FE of 0.16 (0.20) eV in monoclinic (cubic phase) and the formation energy in monoclinic phase turns to negative values at a FE of 4.4 (1.8) eV at O-poor (O-rich) conditions. In cubic phase, the formation energy turns to negative values at a FE of 6.0 (3.6) eV at O-poor (O-rich) conditions. From this we may conclude that Al_{Zr} tends to form negative charge states within the major part of the band gap and further, the Al_{Zr}^{-1} charge state requires compensation by positive charge carriers (holes or defects with positive charge states). The formation of Al_{Zr}^{-1} could increase Al solubility if there are enough defects or carriers of opposite charge available to maintain charge neutrality. The concept of charge neutrality will be discussed in the following section. Under O-rich conditions, Al_{Zr} displays significantly lower formation energy than under O-poor conditions. Al_i undergoes three electronic transitions in monoclinic phase, viz., $(+3|+2)$, $(+2|+1)$, and $(+1|0)$ at FEs of 4.5, 5.0, and 5.7 eV, respectively. In cubic phase Al_{Zr} undergoes transitions $(+3|+2)$ and $(+2|0)$ at FEs of 4.0 and 5.2 eV, respectively. Correcting for DFT band-gap underestimation has a similar effect on Al_i as on V_{O3}, displacing the charge state to considerably higher formation energy and higher Fermi energy. The uncorrected and corrected formation energies as a

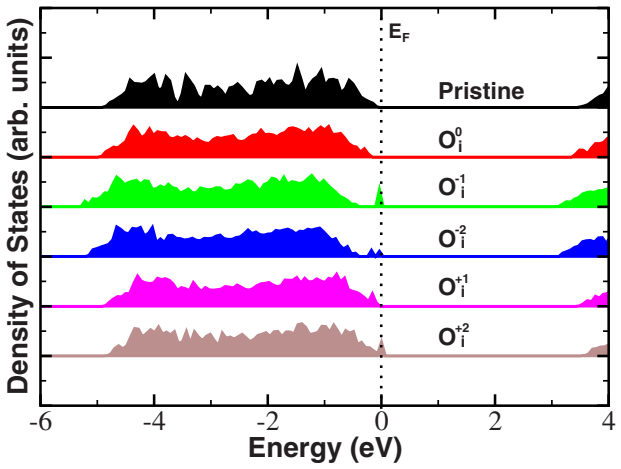

FIG. 5. (Color online) The total density of states for pristine monoclinic ZrO_2 and for monoclinic ZrO_2 with the neutral and charged oxygen interstitial, O_4.

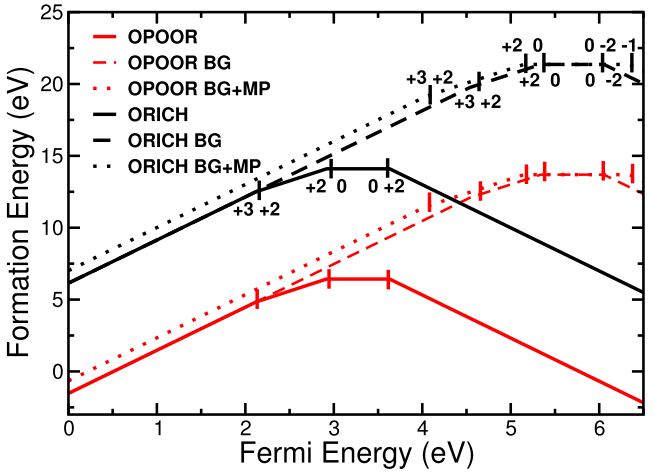

FIG. 6. (Color online) Formation energies as a function of Fermi energy before and after BG and MP correction for interstitial Al in cubic ZrO_2. For clarity the charge state transitions are only marked at oxygen-rich conditions since they will be identical at oxygen-poor conditions.

function of Fermi energy for Al_i in cubic ZrO_2 are displayed in Fig. 6.

From the results of Fig. 4, one can notice that the formation energy of Al_{Zr} can be significantly decreased if the Fermi energy is confined in the region between the middle of the band gap and the bottom of the CB. This could be done by, for instance, introducing a codopant, which compensates for the electron deficiency, which is induced as Al replaces Zr. This codopant should be an extrinsic donor with an effective charge larger than that of Zr, then confining the Fermi energy close to the conduction band. At around this Fermi energy, the energy of Al_{Zr}^{-1} is low and can even attain negative values. It should be pointed out that O_4^{-2} is also low in energy when the Fermi energy is close to the conduction band and might compensate for the introduced codopant, decreasing Al_{Zr}^{-1} concentration. Furthermore, if we expect O_3^{-2} to be lower in energy than O_4^{-2}, as found by Refs. 1, 2, and 13, then the region close to the conduction band, where oxygen interstitials will form spontaneously will be extended. It is then probable that then concentration of Al_{Zr}^{-1} will be somewhat reduced due to compensation of V_{O3}^{+2} by O_3^{-2}. A limiting factor is that the codopant may unintentionally alter not only the electronic but also, for instance, the structural or thermodynamic properties of ZrO_2.

Another possible route to increased Al solubility, which applies to ZrO_2 coatings, could be to grow ZrO_2 on a substrate or growth layer with a suitable band offset with respect to ZrO_2. The position of the VBM of the substrate or growth layer then determines the electron chemical potential of the ZrO_2 coating, lowering the Al formation energy without the need of V_O compensation. In Figs. 4(a) and 4(b), the VBM of Si with respect to monoclinic ZrO_2 is displayed as a dotted line. Growing ZrO_2 on a Si growth layer is likely to confine E_F to energies higher than about 3 eV, a region where Al_{Zr}^{-1} will be low in energy. Moreover, a change in the substrate/growth layer may not only change the electronic structure of ZrO_2 but may also have an effect on its crystallinity and microstructure, and should therefore be chosen with care.

D. Equilibrium defect concentration and Fermi energy

We have calculated the equilibrium defect concentration by using the occupation probability according to the Boltzmann factor, such as

$$c(D^q, E_F, \mu, T) = Ne^{[-\Delta H_f(D^q, E_F, \mu)/k_B T]}, \tag{2}$$

where c is the concentration of defects, N is the concentration of possible defect sites, ΔH_f is the formation energy, μ is the atomic chemical potential, E_F is the Fermi energy or electronic chemical potential, T is the temperature during the crystal-growth process, and k_B is the Boltzmann constant. As discussed above, the atomic chemical potential reflects the crystal-growth conditions and is a variable in this formalism. However, the electronic chemical potential is not a free variable but depends on the concentration of charge defects and free carriers through the charge neutrality condition, which is written as

$$\sum_i^N c_i q_i + n + p = 0, \tag{3}$$

where c_i is the concentration of defects with charge states q_i, n is the concentration of electrons, and p is the concentration of holes. Since, reversibly, c_i, n, and p depends on E_F, the problem of finding E_F, c_i, n, and p was solved self-consistently.[18] We have calculated n and p from the Fermi-Dirac distribution function, approximated by $f_{FD} = e^{\pm(E-E_F)/k_B T}$ (+ for holes and − for electrons), where E is either the electron or hole energy state. The density of states of the electrons and holes have been calculated through an effective mass-like approximation. The effective masses of electrons and holes were $m_e/m_0 = 1.295$ and $m_h/m_0 = 0.32$, respectively.[30] Since, the spread in theoretical data for the effective hole and electron masses is large, we performed benchmark tests to see how the self-consistent Fermi energy is changed by an arbitrary change in these values. A change of up to 50% in electron and/or hole mass does not have any significant influence on the self-consistent Fermi energy (<fourth digit). This is due to the low concentration of carriers (around 10^6 cm^{-3}), common for large band-gap semiconductors or insulators such as ZrO_2.

In Fig. 4, the self-consistently calculated Fermi energies (E_F^{SC}) at 1100 K are marked by vertical dashed lines. In monoclinic phase, at oxygen-poor conditions, E_F^{SC} is pinned very close to the cross point of the Al_{Zr}^{-1} and V_{O3}^{+2} formation energy curves since charge neutrality can be maintained by compensation between these two defects. In cubic phase, also O_4^{-2} intersects around this point, compensating for some of the formed V_{O3}^{+2} and again, E_F^{SC} will be pinned here. At oxygen-rich conditions, the intersections of the Al_{Zr}^{-1} and V_{O3}^{+2} formation energies are quite close to the valence band, making formation of holes increasingly likely. Since, the distance from the calculated E_F^{SC} to the VBM is $\sim k_B T$ at oxygen-rich conditions, the used approximation of the Fermi-Dirac distribution function is not valid in this case and we will hereafter only discuss oxygen-poor conditions. The calculated concentration of Al_{Zr}^{-1} at E_F^{SC} and 1100 was 5.6×10^{16} cm^{-3} in monoclinic phase and 3.2×10^{14} cm^{-3} in cubic phase. This concentration is negligible, corresponding to an atomic percentage of Al in ZrO_2 to less than 1×10^{-5} at. % in monoclinic phase. Indeed, there is little evidence of Al solubility at the given temperature, both at equilibrium and nonequilibrium conditions.[7,8] However, the trend does not follow experiment, where the concentration of Al in monoclinic ZrO_2 is considerably lower than that in the high-temperature phases of ZrO_2. We found an oxygen vacancy concentration of 2.8×10^{16} cm^{-3} in monoclinic phase and of 1.3×10^{14} cm^{-3} in cubic phase. Here as well, the under stoichiometry of oxygen is more pronounced in monoclinic phase than in cubic phase of ZrO_2, which is in contradiction with experimental results. This discrepancy can be explained by the fact that at 1100 K, the cubic phase is not stable under equilibrium conditions and instead, we should consider the relevant temperatures of the stability region of each phase. Thus, we calculated E_F c_i, n, and p self-consistently at the maximum temperature where each phase is still stable, i.e., at

1420 and 2950 K for monoclinic and cubic phases, respectively. The maximum concentrations of Al were then 2.7×10^{18} cm^{-3} in monoclinic phase and 3.4×10^{20} cm^{-3} in cubic phase. The correct experimental trend is now captured, where the concentration of Al in cubic phase is two orders of magnitude higher than that in monoclinic phase, although the absolute values are still too low compared to experimental values; less than 0.0003 at. % in monoclinic phase and less than 0.04 at. % in cubic phase. The corresponding concentration of V_{O3}^{+2} is 1.3×10^{18} cm^{-3} in monoclinic phase and 2.3×10^{20} cm^{-3} in cubic phase. This gives an oxygen content of about 66.6 at. % in cubic ZrO_2 at oxygen-poor conditions. This oxygen vacancy concentration is in the lower limit of experimental findings, where the oxygen content is reported as 61.0–66.7 at. %.[8]

E. Defect interactions

So far Al_{Zr}^{-1} has been found to have the lowest formation energy of all Al-related defects. We have further concluded that Al_{Zr}^{-1} will be compensated by V_{O3}^{+2} and since charge neutrality must be kept, the concentration of V_{O3}^{+2} will be half that of the Al_{Zr} concentration. Therefore, we have decided to study the stability of isolated Al_{Zr} and V_{O3} against the formation of Al_{Zr} in the vicinity of V_{O3}. In order to do that, in addition to the already investigated model systems, we have constructed supercells containing two neutral Al substitutional defects and one O vacancy. First, we have investigated the nature of interaction between these defects by calculating the self-consistent total energy for three different configurations. In the first, both Al_{Zr} defects were nearest neighbors of V_{O3}. In the second, Al_{Zr} were nearest neighbors of each other while V_{O3} was at a distant position. Third, none of the defects were nearest neighbors but at positions as far away as possible, considering the periodicity of the chosen supercell. The first configuration was found to have the lowest energy, leading to the conclusion that Al_{Zr} and V_{O3} display attractive interaction. In fact, the Al-V_{O3}-Al defect cluster is also the next most favorable among the neutral defects, after V_{O3}, with average formation energies of only 0.89 eV (monoclinic) and 0.52 eV (cubic) per defect.

The concentration of Al_{Zr}, assuming that Al-V_{O3}-Al defect clusters form, was calculated at different experimental conditions by the use of Eq. (2), from the formation energy of the defect cluster. The number of possible defect clusters sites, $N_C = \frac{N_{Zr\text{-}Zr}}{2} \times N_{Zr} \times N_O$, were determined by combinatorial analysis for the monoclinic and cubic supercells, respectively. Here, $N_{Zr\text{-}Zr}$ is the Zr-Zr coordination, N_{Zr} is the number of Zr sites, and N_O is the number of common oxygen neighbors to the two Al_{Zr}. In order to eliminate double counting, the Zr-Zr coordination is divided by 2.

The concentrations of Al_{Zr}, as Al-V_{O3}-Al defect clusters form, as a function of temperature in monoclinic and cubic phases are shown in Fig. 7. In the same graph, the concentrations of single Al_{Zr}^{-1} in both phases, calculated self-consistently at a set of temperatures are displayed as symbols. The calculated maximum concentration of Al_{Zr}, coordinated in the Al-V_{O3}-Al defect cluster in cubic phase at 2950 K, is now enhanced by two orders of magnitude, to

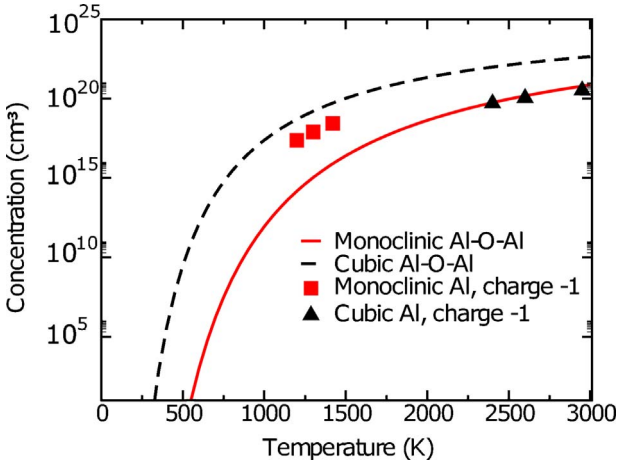

FIG. 7. (Color online) The equilibrium concentration of Al in the Al-V_O-Al defect cluster as a function of temperature in monoclinic(cubic) phase of ZrO_2 is displayed by a solid red (dashed black) line. The symbols represent the self-consistently calculated equilibrium concentration of Al_{Zr}^{-1} in monoclinic and cubic phase at a few different temperatures. The red squares correspond to Al_{Zr}^{-1} concentration in monoclinic phase and the black triangles correspond to the Al_{Zr}^{-1} concentration in cubic phase.

4.0×10^{22} cm^{-3} (~5 at. %), well within experimental values.[8] The concentration of V_{O3} will be half the concentration of Al, 2.0×10^{22} cm^{-3}. This gives an oxygen content of ~64 at. %, in excellent agreement with experiment.[8] In monoclinic phase, the maximum concentration of Al as Al-V_{O3}-Al clusters are allowed to form is negligible at 1420 K, 4.0×10^{15} cm^{-3}. We conclude that if Al_{Zr} is accompanied by V_{O3}, forming Al-V_{O3}-Al defect clusters, the experimental concentrations of both defects and in both phases are very well represented by our calculated values.

IV. CONCLUSIONS

First-principles theory, using the supercell approach, has been employed to investigate the energetics of Al and intrinsic defects in the monoclinic and cubic phases of ZrO_2. We find that V_{O3}^0 is the most stable isolated neutral defect and that Al_{Zr}^0 will be lower in formation energy than Al_i^0. Among the intrinsic defects, Zr_i^0 and V_{Zr}^0 are the highest in energy. We have performed corrections for defect-defect interactions and for the DFT underestimation of the band gap. From the analysis of the defect formation energy as a function of Fermi energy, we find that the charge transition states of O_4 and V_{O3}, without band-gap correction, are in close agreement with the results available from literature, as are the formation energies of the neutral defects. As the Fermi energy is increased, Al_{Zr}^0 decays into the Al_{Zr}^{-1} charge state, which will be compensated by V_{O3}^{+2}. From this we find that the formation energy of Al_{Zr} can be significantly decreased if the Fermi energy is confined in the region between the middle of the band gap and the bottom of the CB. This could be done, for instance, by introducing codopants or growing ZrO_2 on a substrate or growth layer with a suitable band offset. By calculating the self-consistent Fermi energy of each system

and at different temperatures, we could estimate the equilibrium concentrations of all relevant defects. At the self-consistently calculated Fermi energy, Al_{Zr}^{-1} and V_{O3}^{+2} have the highest concentration. The calculated maximum equilibrium concentration of Al_{Zr}^{-1} captures the correct experimental trend but underestimates experimental data, as does the concentration of V_{O3}^{+2}. The interaction between Al_{Zr}^{-1} and V_{O3}^{+2} was considered by modeling both defects in the same supercell in the concentrations required by the condition of charge neutrality. We show that the formation energy of Al-V_{O3}-Al defect clusters from Al_{Zr}^{0} and V_{O3}^{0} is the second lowest among the neutral defects. The calculated concentrations of Al_{Zr}^{0} and V_{O3}^{0}, as Al-V_{O3}-Al defect clusters are assumed to form, are in very good quantitative agreement with the concentrations of Al and oxygen vacancies found in experiment. Our results suggest that defect clusters will form as a result of Al doping in cubic phase of ZrO_2, whereas the concentration of defect clusters is negligible in the monoclinic phase, both in accordance with experiment.[31]

ACKNOWLEDGMENTS

We would like to acknowledge the Swedish Research Council and Sandvik Tooling, Sweden for the funding of this project. We would also like to acknowledge Susanne Norgren, Sandvik Tooling, Sweden, David Andersson, LANL, U.S.A. for discussions on thermodynamics of these systems, Jolla Kullgren, Department of Materials Chemistry, Uppsala University, Sweden for development of a script for finding interstitial positions, and finally we would like to thank Johan Björklund, Department of Mathematics, Uppsala University for his help within the area of combinatorial analysis.

[1] A. S. Foster, V. B. Sulimov, F. Lopez Gejo, A. L. Shluger, and R. M. Nieminen, J. Non-Cryst. Solids **303**, 101 (2002).
[2] A. S. Foster, V. B. Sulimov, F. Lopez Gejo, A. L. Shluger, and R. M. Nieminen, Phys. Rev. B **64**, 224108 (2001).
[3] M. Chen, B. Hallstedt, and L. J. Gauckler, Solid State Ionics **170**, 255 (2004).
[4] C. Bjormander, Surf. Coat. Technol. **201**, 4032 (2006).
[5] P. Martensson, Surf. Coat. Technol. **200**, 3626 (2006).
[6] O. Vasylkiv, Y. Sakka, and V. V. Skorokhod, Mater. Trans. **44**, 2235 (2003).
[7] D. H. Trinh, J. M. Andersson, M. Collin, I. Reineck, U. Helmersson, and L. Hultman, J. Vac. Sci. Technol. A **24**, 309 (2006).
[8] O. Fabrichnaya and F. Aldinger, Z. Metallkd. **95**, 27 (2004).
[9] S. Popovic, G. Stefanic, and S. Music, Mater. Lett. **31**, 19 (1997).
[10] A. M. Alper, Science of Ceramics **3**, 339 (1967).
[11] S. Moreau, M. Gervais, and A. Douy, Solid State Ionics **101-103**, 625 (1997).
[12] G. Stefanic, S. Music, and R. Trojko, J. Alloys Compd. **388**, 126 (2005).
[13] J. X. Zheng, G. Ceder, T. Maxisch, W. K. Chim, and W. K. Choi, Phys. Rev. B **75**, 104112 (2007).
[14] G. Kresse and J. Hafner, Phys. Rev. B **47**, 558 (1993).
[15] J. P. Perdew, J. A. Chevary, S. H. Vosko, K. A. Jackson, M. R. Pederson, D. J. Singh, and C. Fiolhais, Phys. Rev. B **46**, 6671 (1992); Phys. Rev. B **48**, 4978 (1993)
[16] J. P. Perdew and Y. Wang, Phys. Rev. B **45**, 13244 (1992).
[17] R. W. G. Wyckoff, *Crystal Structures* (Wiley, New York, 1963), Vol. 1.
[18] C. Persson, Y.-J. Zhao, S. Lany, and A. Zunger, Phys. Rev. B **72**, 035211 (2005).
[19] C. G. Van De Walle and Jörg Neugebauer, J. Appl. Phys. **95**, 3851 (2004).
[20] D. A. Andersson, S. I. Simak, B. Johansson, I. A. Abrikosov, and N. V. Skorodumova, Phys. Rev. B **75**, 035109 (2007).
[21] G. Makov and M. C. Payne, Phys. Rev. B **51**, 4014 (1995).
[22] R. H. French, S. J. Glass, F. S. Ohuchi, Y. N. Xu, and W. Y. Ching, Phys. Rev. B **49**, 5133 (1994).
[23] J. P. Perdew, K. Burke, and M. Ernzerhof, Phys. Rev. Lett. **77**, 3865 (1996)
[24] David R. Lide, *CRC Handbook of Chemistry and Physics* (CRC, Cleveland, 2008).
[25] G. Jomard, T. Petit, A. Pasturel, L. Magaud, G. Kresse, and J. Hafner, Phys. Rev. B **59**, 4044 (1999).
[26] C. J. Howard, R. J. Hill, and B. E. Reichert, Acta Crystallogr., Sect. B: Struct. Sci. **44**, 116 (1988).
[27] R. W. G. Wyckoff, *Crystal Structures*, 2nd ed. (Wiley, New York, 1964), Vol. 274.
[28] H. d'Amour, D. Schifer, W. Denner, H. Schulz, and W. B. Holzapfel, J. Appl. Phys. **49**, 4411 (1978).
[29] D. Nagle, V. R. Paiverneker, A. N. Petelin, and G. Groff, Mater. Res. Bull. **24**, 619 (1989).
[30] A. V. Shaposhnikov, D. V. Gritsenko, I. P. Petrenko, O. P. Pchelyakov, V. A. Gritsenko, S. B. Érenburg, N. V. Bausk, A. M. Badalyan, Yu. V. Shubin, T. P. Smirnova, H. Wong, and C. W. Kim, J. Exp. Theor. Phys. **102**, 799 (2006).
[31] M. Hillert, J. Am. Ceram. Soc. **74**, 2005 (1991).